Behavioral/Systems/Cognitive

The HVC Microcircuit: The Synaptic Basis for Interactions between Song Motor and Vocal Plasticity Pathways

Richard Mooney and Jonathan F. Prather

Department of Neurobiology, Duke University School of Medicine, Durham, North Carolina 27710

Synaptic interactions between telencephalic neurons innervating descending motor or basal ganglia pathways are essential in the learning, planning, and execution of complex movements. Synaptic interactions within the songbird telencephalic nucleus HVC are implicated in motor and auditory activity associated with learned vocalizations. HVC contains projection neurons (PNs) (HVC_{RA}) that innervate song premotor areas, other PNs (HVC_X) that innervate a basal ganglia pathway necessary for vocal plasticity, and interneurons (HVC_{INT}). During singing, HVC_{RA} fire in temporally sparse bursts, possibly because of HVC_{INT}–HVC_{RA} interactions, and a corollary discharge can be detected in the basal ganglia pathway, likely because of synaptic transmission from HVC_{RA} to HVC_X cells. During song playback, local interactions, including inhibition onto HVC_X cells, shape highly selective responses that distinguish HVC from its auditory afferents. To better understand the synaptic substrate for the motor and auditory properties of HVC, we made intracellular recordings from pairs of HVC neurons in adult male zebra finch brain slices and used spike-triggered averages to assess synaptic connectivity. A major synaptic interaction between the PNs was a disynaptic inhibition from HVC_{RA} to HVC_X, which could link song motor signals in the two outputs of HVC and account for some of the song playback-evoked inhibition in HVC_X cells. Furthermore, single interneurons made divergent connections onto PNs of both types, and either PN type could form reciprocal connections with interneurons. In these two regards, the synaptic architecture of HVC resembles that described in some pattern-generating networks, underscoring features likely to be important to singing and song learning.

Key words: HVC; *in vitro* intracellular; paired recordings; zebra finch; songbird; GABA$_A$; picrotoxin; unitary synaptic coupling

Introduction

Identifying synapses in the vertebrate telencephalon that link neurons in primary motor pathways with neurons in basal ganglia pathways is important to an understanding of motor learning, planning, and execution. Songbirds learn to sing via audition-dependent vocal plasticity (Konishi, 1965; Price, 1979), and the songbird telencephalic sensorimotor nucleus HVC contains different projection neurons (PNs) that give rise to either a premotor pathway specialized for song patterning or a basal ganglia pathway necessary for audition-dependent vocal plasticity (see Fig. 1) (Nottebohm et al., 1976, 1982; Fortune and Margoliash, 1995; Foster and Bottjer, 1998; Brainard and Doupe, 2000). These features make HVC an essential site to probe for synaptic interactions important to singing and song learning.

Neurons in HVC comprise at least three major types, including PNs (HVC_{RA}) that gives rise to a descending premotor pathway obligatory for song, other PNs (HVC_X) that innervate a basal ganglia structure within an anterior forebrain pathway (AFP) essential to vocal plasticity, and interneurons (HVC_{INT}) (see Fig.

1) (Kirn et al., 1991; Johnson and Bottjer, 1993; Mooney, 2000). All three cell types extend axonal processes within HVC, affording the means for local synaptic processing (Katz and Gurney, 1981; Mooney, 2000). Several findings suggest that synaptic processing in HVC is extensive and likely to have important behavioral consequences, given the connections of HVC with premotor areas and the AFP. First, HVC_{RA} neurons generate temporally sparse, high-frequency action potential bursts during singing (Hahnloser et al., 2002), and these bursts could propagate through the HVC_{RA} ensemble via local excitatory connections and be terminated by local inhibitory interneurons. Second, AFP neurons display song motor activity (Hessler and Doupe, 1999), and this putative corollary discharge could arise because of coupling between premotor (HVC_{RA}) and HVC_X neurons (Troyer and Doupe, 2000). Finally, HVC neurons exhibit highly selective action potential responses to playback of the bird's own song (BOS), and certain features of these responses, including their temporal sparseness and sensitivity to specific syllable sequences, are thought to be refined by local circuit interactions in HVC (Margoliash, 1983; Margoliash and Fortune, 1992; Lewicki, 1996; Theunissen and Doupe, 1998; Mooney, 2000; Coleman and Mooney, 2004). Indeed, *in vivo* intracellular recordings show that BOS playback evokes distinct subthreshold responses and reciprocal firing patterns in the two PNs and that hyperpolarizing inhibition sculpts BOS-evoked firing patterns in HVC_X cells, suggestive of interneuron–PN interactions (Mooney, 2000; Rosen and Mooney, 2003).

Table 1. Frequency of cell pairs encountered in HVC

Pair type	Number of pairs (percentage of total)	Number of connected pairs (percentage of pairs) [percentage total pairs]	Type of interaction (number of observations)
HVC$_{RA}$–HVC$_X$	46 (47.9)	6 (13) [6.25]	HVC$_{RA}$–HVC$_X$ IPSP (4) HVC$_X$–HVC$_{RA}$ dPSP (5) HVC$_X$–HVC$_{RA}$ IPSP (1) Three reciprocally connected pairs
HVC$_X$–HVC$_X$	19 (19.8)	5 (26.3) [5.21]	All unidirectional IPSPs
HVC$_{INT}$–HVC$_X$	12 (12.5)	3 (25) [3.12]	HVC$_{INT}$–HVC$_X$ IPSP (2) HVC$_X$–HVC$_{INT}$ dPSP (1) One reciprocally connected pair
HVC$_{RA}$–HVC$_{RA}$	9 (9.4)	1 (11.1) [1]	Unidirectional dPSP
HVC$_{RA}$–HVC$_{INT}$	6 (6.2)	2 (33) [2]	HVC$_{INT}$–HVC$_{RA}$ IPSP (1) HVC$_{INT}$–HVC$_{RA}$ dPSP (1)
HVC$_{INT}$–HVC$_{INT}$	4 (4.2)	1 (25) [1]	Unidirectional IPSP
Total	96 (100%)	18 (18.7) [NA]	

Although the motor and auditory properties of HVC hint at extensive local processing, knowledge of the synaptic interactions between identified HVC neuron types remains incomplete. This gap in understanding exists because axonal and dendritic processes from all three cell types as well as axonal processes from HVC afferents are interwoven with each other, complicating analysis of intrinsic connectivity (Nixdorf, 1989; Fortune and Margoliash, 1995; Foster and Bottjer, 1998; Mooney, 2000). We made intracellular recordings from pairs of identified HVC neurons in brain slices and calculated spike-triggered averages (STAs) (Perkel et al., 1967) to assess synaptic connections. We also antidromically stimulated HVC$_{RA}$ neurons and applied neurotransmitter receptor blockers to further characterize the intrinsic connectivity of HVC. We found extremely robust disynaptic feedforward inhibition from HVC$_{RA}$ to HVC$_X$ neurons, which may influence how HVC shapes and conveys song motor activity to the AFP and could account for the contrasting BOS-evoked responses in the different PNs. In addition, single interneurons can contact multiple PNs, and interneurons and PNs can form reciprocal connections. Similar architectural features contribute to synchronous oscillations in other pattern-generating networks (Selverston and Moulins, 1985) and have implications for the role of HVC in song patterning. Some results have been published in abstract form (Prather and Mooney, 2003).

Materials and Methods

These experiments use electrophysiological techniques that have been described extensively in previous published studies (Mooney, 1992; Livingston and Mooney, 1997; White et al., 1999; Livingston et al., 2000). Therefore, only a brief description of these techniques is provided here.

Subjects. Thirty-nine adult male zebra finches (>120 d posthatch) were used for these experiments, in accordance with a protocol approved by the Duke University Institutional Animal Care and Use Committee. Finches were raised in our breeding colony on a 14/10 h light/dark cycle.

Brain slices. After induction of inhalation anesthesia (halothane), the bird was decapitated, and the brain was removed rapidly and placed in oxygenated ice-cold artificial CSF (ACSF). Sagittal brain slices that included HVC were cut at 400–500 μm thickness and transferred to a holding chamber (room temperature) for 2–4 h. Individual slices were transferred to an interface-type chamber (30°C; Medical Systems, Greenvale, NY) for intracellular recordings. The ACSF consisted of (in mM) 119 NaCl, 2.5 KCl, 1.3 MgCl$_2$, 2.5 CaCl$_2$, 1 NaH$_2$PO$_4$, 26.2 NaHCO$_3$, and 11 glucose, equilibrated with 95%O$_2$/5%CO$_2$. Equiosmolar sucrose was substituted for NaCl during the tissue preparation stage.

Electrophysiological recordings. Sharp intracellular recordings were made with borosilicate glass pipettes (Sutter Instruments, Novato, CA) pulled to a final resistance of 80–200 MΩ when filled with 2 M potassium acetate and 5% Neurobiotin (Vector Laboratories, Burlingame, CA). In a few experiments, one of the two recording electrodes contained 5% Lucifer yellow (LY) in a 1 M lithium chloride solution. Cell penetration was achieved by briefly "ringing" the electrode using capacitance overcompensation, and the cell was then stabilized by passing regular hyperpolarizing current pulses through the recording electrode (−0.5 nA, 500 ms at 1 Hz). Intracellular potentials were amplified with an Axoclamp 2B amplifier (Axon Instruments, Union City, CA) in bridge mode, low-pass filtered at 1–3 kHz, and digitized at 10 kHz. To make paired recordings, we first obtained a stable recording from an HVC neuron and then lowered the second recording electrode to a point typically within ∼50 μm of the first electrode and searched for its synaptic partners. This search strategy tended to favor finding pairs in which the first cell obtained was of a type affording a more stable recording, which in our hands tended to be the HVC$_X$ cell type (Table 1) (see Results). Synaptically coupled cells usually could be identified on-line by the appearance of a hyperpolarizing or depolarizing response in one cell locked to the action potential discharge of the other cell, and also by subsequent on-line analysis of STAs (see below). Synaptically coupled cell pairs were most often encountered when the two electrode tips were in close (∼50 μm) proximity to one another, and although a detailed count of unconnected pairs was not kept for all experiments, ∼10–20% of cell pairs showed evidence of unidirectional or bidirectional synaptic coupling.

Electrophysiological data acquisition and analysis. Data acquisition and analysis for single and paired intracellular recordings were performed using a data acquisition board (AT-MIO-16E2; National Instruments, Austin, TX), controlled by custom Labview software developed by Fred Livingston, Rob Neummann, and Merri Rosen (Duke University, Durham, NC). In paired recordings, one or two action potentials were elicited in turn from each neuron in the pair by passing brief (∼10 ms) depolarizing current pulses (+0.5 to 1 nA) through the recording electrode. A software threshold peak detector was used to generate STAs of the membrane potential of the partner cell in the pair. In most cases, current amplitudes and/or the resting membrane potential of the trigger cell were adjusted to elicit only a single action potential per pulse, but in a few cells, two or three spikes were sometimes evoked. In these cases, the STA was calculated off the first spike in the series. STAs were plotted in reference to the time of the trigger spike; note that the zero time for the STA corresponds to the action potential peak and that we suspect that the resultant STAs might be slightly leftward-shifted with respect to the actual onset of transmitter release (see Fig. 5B). After collecting 10–40 pulse trials per cell, we then conducted further characterizations of the impaled cells, including their responses to more prolonged depolarizing currents (0.5 s at +0.5 nA). All HVC neurons in this study were identified to type based on their DC-evoked properties, as described previously (Dutar et al., 1998; Mooney, 2000). Briefly, HVC$_{RA}$ neurons fire only one to several action potentials to +0.5 nA currents of 0.5 s duration, whereas HVC$_X$ neurons fire more regularly with moderate spike-frequency adaptation, and HVC$_{INT}$ fire at high frequency with little or no spike-frequency adaptation (see Fig. 1D). In addition, HVC$_{INT}$ can be distinguished from HVC PNs by their narrower spike widths (∼1 vs 2 ms) (Mooney, 2000; Rauske et al., 2003). In many cases, at least one cell in the pair was confirmed to morphological type through intracellular staining and *post hoc* morphological visualization. Relatively brief recording times (<15 min) prevented thorough filling of both cells in the recorded pair in all but a few cases.

In a subset of paired recordings from synaptically coupled cells, and in all cases in which we recorded from either a single cell or unconnected pairs for pharmacological experiments (see below), we also antidromically activated HVC$_{RA}$ neurons, and thus their axon collaterals within HVC, by passing currents (∼25–100 μA for 100 μsec) from an Isolator-10 stimulus isolation unit (Axon Instruments) to the HVC fibers

that project to the robust nucleus of arcopallium (RA), using a concentric bipolar stimulating electrode (FHC, Brunswick, ME) placed midway between HVC and RA in the region of the caudal telencephalon. HVC axons innervating RA are clearly visible in the brain slice under epi-illumination, appearing as large braids of whitish fibers (see Fig. 1A). Anatomical studies suggest that these fiber braids are composed exclusively of HVC_{RA} axons, although a few HVC_X axons do travel medial to this area but outside the plane of the slices used here (Mooney, 2000). This mid-point placement was chosen because it is unlikely to activate axons of HVC afferents. Furthermore, antidromic activation of HVC_{RA} neurons was confirmed in some recordings by the appearance of an action potential riding on the shoulder of the stimulus artifact itself. In contrast, as HVC_X axons exit rostrally and ventrally from the nucleus, they intermingle with axons arising from several afferents of HVC (i.e., NIf, Uva, and mMAN). This organization renders selective recruitment of HVC_X axon collaterals by extracellular stimulation in the brain slice unlikely, and thus we did not attempt to use an antidromic stimulation approach to activate HVC_X axon collaterals. Instead, we relied solely on paired recordings to deduce the nature of the synaptic connectivity that HVC_X neurons make with the other HVC neuron types.

Several different features of the STA were characterized off-line, including the peak amplitude, the time to peak, and the 25% rise time (i.e., the time to reach 25% of the peak amplitude). In the small minority of cases in which the trigger neuron spiked repetitively and the STA demonstrated a biphasic peak, the first peak was used for these measurements. An ANOVA was used to compare a given STA feature across different cell pair types, followed by Tukey's *post hoc* test corrected for multiple comparisons. Values reported are the mean ± SEM, unless noted otherwise.

Synaptic pharmacology. To analyze the types of postsynaptic receptors activated either after antidromic stimulation of HVC_{RA} neurons or in the case of some synaptically coupled pairs, drugs were bath applied to the whole slice after collecting evoked synaptic responses for a 5–10 min baseline period. Picrotoxin (PTX; 50 μM) was used to block inhibitory receptors of the $GABA_A$ subtype, whereas D(−)-2-amino-5-phophonopentanoic acid (D-APV; 50 μM) was used to block excitatory transmission mediated by NMDA receptors and 1,2,3,4-tetrahydro-6-nitro-2,3-dioxo-benzo(*f*)quinoxaline-7-sulfonamide disodium (NBQX; 10 μM) was used to block fast excitatory transmission mediated by ionotropic glutamate receptors of the AMPA subtype. The use of an interface chamber, which we prefer for its superior slice viability compared with submersion chambers, especially when recording above room temperature, precluded collecting washouts in most cases (i.e., washout times greatly exceeded 1 h). We used other features, such as the maintenance of excitatory transmission in the presence of PTX, as well as resting membrane potential and input impedance, to determine that synaptic blockade did not reflect a general rundown of the cell or the slice. Drug effects were assessed using paired or unpaired *t* tests, as appropriate for normally distributed data, and a Mann–Whiney *U* test for other data sets.

Intracellular staining and imaging. After acquiring electrophysiological data, Neurobiotin was iontophoresed into the cell with positive current pulses (+0.5 to 1 nA, 500 ms per second, for ~15 min). For LY staining, negative current pulses were passed through the electrode (−1 nA, 500 ms at 1 Hz). Slices then were fixed in 4% paraformaldehyde in 25 mM sodium phosphate buffer (PB) overnight at 4°C and then sunk in 30% sucrose in 25 mM PB. Slices then were resectioned at 75–100 μm thickness on a freezing microtome, and Neurobiotin was visualized with a standard avidin–fluorophore reaction using a 1:1000 dilution of avidin–Alexa Fluor 488 or 564 (Molecular Probes, Eugene, OR). Confocal images were generated with a Zeiss (Thornwood, NY) 510 laser scanning microscope, using either a 40× [1.3 numerical aperture (NA)] or 63× (1.4 NA) Zeiss NeoFluar objective and rhodamine/fluorescein filters [488 and 543 nm excitation wavelengths, emission bandpass filter of 500–540 nm, and emission long-pass filter of 560, sampled in an alternating frame arrangement; optical sections of 1 Airey unit (~1 μm thickness), with Kalman averaging = 2].

Parvalbumin immunoreactivity. In some experiments, we combined intracellular staining with Neurobiotin and immunohistochemical methods to determine which cells in HVC were positive for parvalbumin

(PV), a calcium-binding protein previously localized to HVC interneurons (Wild et al., 2005). After cell fills, brain slices were transferred to 4% paraformaldehyde within 30 min, where they remained for a minimum of 24 h before being placed in 30% sucrose for several hours and then sectioned at 50 μm on a freezing microtome. The sections were then incubated in streptavidin–Alexa Fluor 488 in PBS–Triton X-100 overnight, washed in PBS, and incubated overnight again with anti-PV antibody (mouse monoclonal; Swant, Bellinzona, Switzerland) at a dilution of 1:500. All immunohistochemical reactions were performed on free-floating sections at room temperature in PBS containing 0.4% Triton X-100 (PBS-TX). Primary antibody incubations were performed overnight with the inclusion of 2.5% normal horse serum and 0.1% sodium azide. PV was visualized using a biotinylated horse anti-mouse antibody (Vector Laboratories), followed by streptavidin–Alexa Fluor 564 (Molecular Probes). Secondary antibody incubations were 1–2 h in duration in PBS-TX. Between treatments, the sections were washed thoroughly in PBS.

Results

We used blind dual sharp microelectrode recording techniques to record from synaptically coupled pairs of cells in the telencephalic song nucleus HVC (Fig. 1A,B). Previous *in vitro* and *in vivo* studies have shown that in addition to their morphological differences, HVC_{RA}, HVC_X, and HVC_{INT} are readily distinguished from each other based on their DC-evoked firing properties (Dutar et al., 1998; Mooney, 2000). In the present study, we identified all cells by their DC-evoked action potential responses and/or intracellular staining with Neurobiotin and *post hoc* visualization (Fig. 1C,D) (see Materials and Methods). Synaptic potentials were evident as depolarizing or hyperpolarizing membrane potential responses in one of the cells immediately after the spontaneous and/or DC-evoked action potentials of the other cell. With respect to both raw and averaged membrane potential records, we refer to spike-evoked responses that are hyperpolarizing as IPSPs, depolarizing responses as dPSPs, and depolarizing responses that demonstrably evoked spiking in the postsynaptic cell as EPSPs. In all cases, action potentials were evoked in turn from each of the cells in the pair, allowing us to assess synaptic coupling in both directions. In total, we found 79 neuron pairs that exhibited evidence of either unidirectional or bidirectional synaptic coupling, including 29 HVC_{RA}–HVC_X pairs, 20 HVC_{INT}–HVC_X pairs, 13 HVC_{RA}–HVC_{INT} pairs, 11 HVC_X–HVC_X pairs, 5 HVC_{RA}–HVC_{RA} pairs, and 1 HVC_{INT}–HVC_{INT} pair (*n* = 53 slices from 30 birds). In this study, the relative abundance of connected neuronal pairs of a given class is dependent on both the true probability of connections within that class and the probability of sampling from that class. Therefore, the major focus of these results is on describing the nature of connections in each class of paired cells rather than the relative prevalence of connections among the different classes.

HVC_{RA}–HVC_X pairs

A total of 29 HVC_X–HVC_{RA} neuronal pairs exhibited evidence of synaptic coupling. In almost all (26 of 29) pairs of synaptically coupled HVC_{RA}–HVC_X neurons, DC-evoked action potentials in the HVC_{RA} neuron triggered a synaptic response in the HVC_X neuron. In the vast majority of these cases, action potentials in the HVC_{RA} neuron evoked an IPSP in the HVC_X cell (Fig. 2A, Table 2) (25 of 26 cases evoked IPSPs; 1 of 26 cases evoked a dPSP). The amplitudes of these HVC_{RA}–HVC_X IPSPs often were sufficiently large (>1 mV) to be visible without averaging. HVC_{RA} STAs (see Materials and Methods) of the HVC_X neuronal membrane potential had an average peak amplitude of −1.5 ± 0.3 mV, an average time to peak of 15.7 ± 1.0 ms, and a 25% rise time of 4.8 ± 0.4 ms (*n* = 25) (Fig. 2B, Table 2).
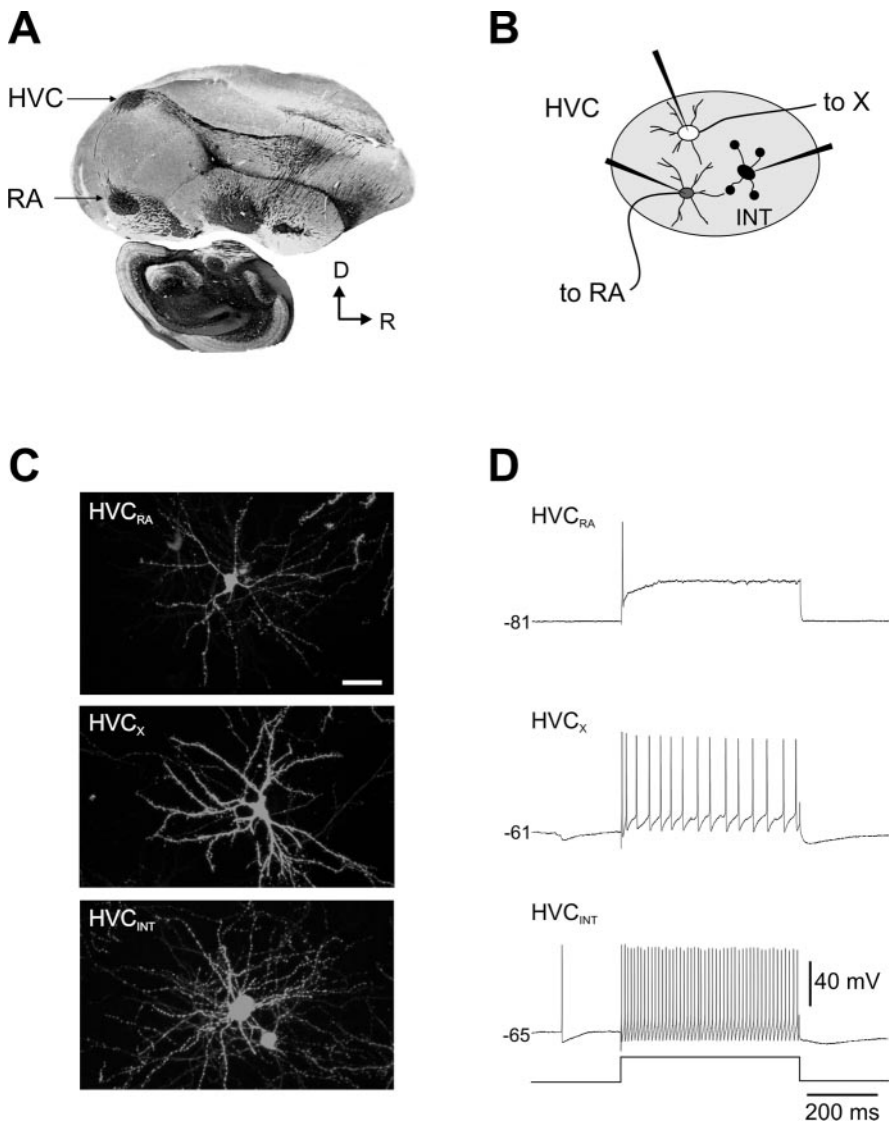
Figure 1. The song nucleus HVC in the zebra finch telencephalon contains two different classes of PN and at least one class of interneurons. ***A***, A sagittal section through the telencephalon of an adult male zebra finch, stained for myelin, showing the song nucleus HVC and one of its two efferent targets, the song premotor nucleus RA. HVC fibers transiting to RA can be seen between the two nuclei. Area X, the other efferent target of HVC, is medial to this plane of section. D, Dorsal; R, rostral. ***B***, A schematic of the song nucleus HVC, showing the three neuron classes, including PNs that innervate RA (HVC$_{RA}$), PNs that innervate Area X (HVC$_X$), and interneurons. Simultaneous dual electrode recordings were made from different pairs of HVC neurons to study their synaptic connectivity. ***C***, Confocal images of the three HVC neuron types studied here, as revealed by intracellular staining with Neurobiotin and *post hoc* visualization with avidin–Alexa Fluor 488 (see Materials and Methods). HVC$_{RA}$ neurons (top) possessed slender and sparsely spinous dendrites and elaborated a main axon that exited at the caudal margin of HVC. HVC$_X$ neurons (middle) were characterized by thicker and more spinous dendrites and an axon that exited HVC along its rostroventral border. Interneurons (bottom) were characterized by aspinous, varicose dendrites and lacked an axon that exited HVC. Scale bar, 20 μm. ***D***, Typical membrane potential responses of the three HVC neuron types to depolarizing current pulses (bottom trace). HVC$_{RA}$ neurons (top trace) fired only one or a few action potentials, even in response to large-amplitude depolarizing currents (+1.5 nA). HVC$_X$ neurons (middle trace) fired repetitively to moderate currents (+0.5 nA) with some spike-frequency accommodation. Interneurons (HVC$_{INT}$) fired at high frequencies with little or no spike-frequency accommodation in response to moderate depolarizing current (+0.5 nA). Action potential widths of interneurons are narrower than in either of the PN types (data not shown). Resting potentials (in millivolts) are shown to the left of each membrane potential trace.

Synaptic coupling from HVC$_X$ to HVC$_{RA}$ neurons was detected less frequently. In 7 of 29 pairs of synaptically coupled HVC$_{RA}$–HVC$_X$ neurons, action potentials in the HVC$_X$ cell triggered synaptic responses in HVC$_{RA}$ neurons. In four of these cases, action potentials in the HVC$_X$ neuron evoked a dPSP in the HVC$_{RA}$ cell, whereas in the other three cases, IPSPs were elicited (Table 2). Notably, reciprocal connections were detected in 5 of

the 29 pairs of synaptically coupled HVC$_{RA}$–HVC$_X$ neurons (data not shown). In all of these cases, action potentials in the HVC$_{RA}$ neuron evoked IPSPs in the HVC$_X$ cell; HVC$_X$ cell action potentials evoked dEPSPs in three of these pairs and IPSPs in the other two pairs. These results indicate that bidirectional synaptic interactions, including reciprocal inhibitory interactions, can occur between HVC$_{RA}$ and HVC$_X$ neurons. Furthermore, these recordings suggest that a dominant pattern of synaptic connectivity between the two HVC PNs involves inhibition from HVC$_{RA}$ to HVC$_X$ neurons.

We suspected that the inhibitory interaction between HVC$_{RA}$ and HVC$_X$ neurons was mediated by interposed interneurons, given that HVC$_{RA}$ neurons are known to evoke ionotropic glutamate receptor-mediated EPSPs in neurons in the song nucleus RA (Mooney and Konishi, 1991). In this model, the local collaterals of HVC$_{RA}$ neurons excite inhibitory interneurons via ionotropic glutamatergic synapses, which in turn make inhibitory synapses on HVC$_X$ neurons. Consistent with the disynaptic model, both the mean 25% rise time and the mean time to peak of IPSPs in HVC$_{RA}$–HVC$_X$ cell pairs were significantly longer than those of the IPSPs evoked in HVC$_X$ cells by interneurons (see Table 2 for statistical comparisons and the following discussion of synaptic coupling in HVC$_{INT}$–HVC$_X$ cells pairs) (see also Fig. 5*B*). Furthermore, in some HVC$_{RA}$–HVC$_X$ cell pairs, hyperpolarizing responses in HVC$_X$ neurons only were evoked when the HVC$_{RA}$ neuron fired a spike doublet or triplet, possibly reflecting facilitation at an intervening excitatory synapse (Fig. 2*C*) ($n = 2$ cases). These observations provide indirect evidence that HVC$_{RA}$ cells evoke IPSPs in HVC$_X$ neurons via a disynaptic mechanism. Another possibility is that the axon collaterals of HVC$_{RA}$ neurons provide monosynaptic inhibition onto HVC$_X$ neurons, perhaps via the hyperpolarizing metabotropic glutamate receptors that have been detected within HVC (Schmidt and Perkel, 1998; Dutar et al., 1999, 2000). This monosynaptic model is less likely, given that metabotropic forms of synaptic transmission typically exhibit a much slower onset than observed here for HVC$_{RA}$–HVC$_X$ cell pairs.

These two models can be distinguished by pharmacological methods: HVC$_{RA}$-evoked IPSPs in HVC$_X$ neurons mediated by the disynaptic mechanism will be abolished by ionotropic glutamate receptor blockers, whereas IPSPs mediated by a monosynaptic, metabotropic glutamatergic pathway should not be affected by such treatment. To distinguish between these two outcomes, we recorded intracellularly from HVC$_X$ cells and an-

A

B

C
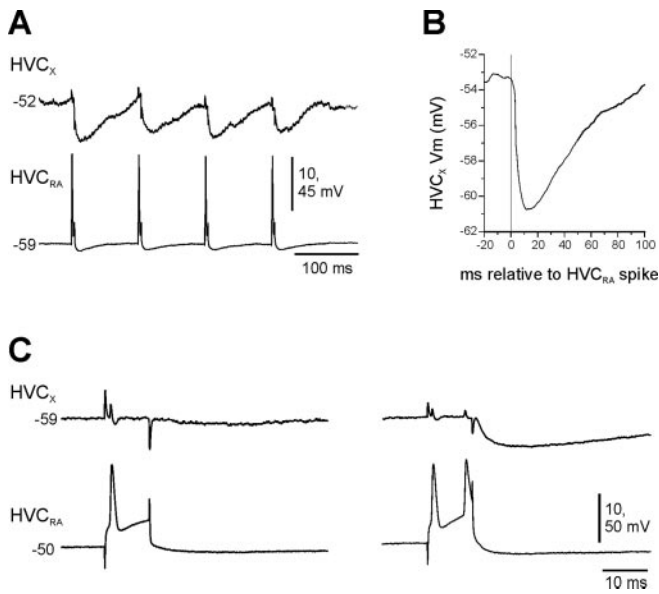
Figure 2. Action potentials in HVC_{RA} neurons evoke IPSPs in HVC_X neurons. *A*, Dual intracellular recordings show that DC-evoked action potentials in the HVC_{RA} neuron (bottom trace) can evoke IPSPs in the HVC_X neuron. *B*, An HVC_{RA} STA of the HVC_X neuron membrane potential, plotted relative to the HVC_{RA} action potential peak (0 ms; positive times follow the action potential), for the cell pair shown in *A*. A membrane hyperpolarization followed the HVC_{RA} action potential, indicating that HVC_{RA} neurons directly or indirectly drive IPSPs in the HVC_X cell. *C*, In some HVC_{RA}–HVC_X cell pairs, spike doublets in the HVC_{RA} neuron were necessary to drive IPSPs in the HVC_X cell (right traces), whereas single spikes failed to evoke any response (left traces), suggestive of disynaptic coupling.

tidromically activated HVC_{RA} axon collaterals *en masse* and then bath applied ionotropic glutamate receptor blockers to the slice (Fig. 3). In control conditions, antidromic stimulation of HVC_{RA} axons evoked robust IPSPs in all HVC_X neurons that we tested ($n = 5$), and in all cases, these IPSPs were abolished by the bath application of a mixture of ionotropic glutamate receptor blockers, NBQX (10 μM) and D-APV (50 μM) (Fig. 3) (mean ± SD: control, −12.4 ± 4.8 mV; drug, 0.9 ± 1.7 mV; paired *t* test; $n = 5$; $p = 0.00132$). These results support a model in which HVC_{RA} axon collaterals activate excitatory ionotropic glutamate receptors on inhibitory interneurons, ultimately providing a disynaptic inhibitory linkage from HVC_{RA} to HVC_X cells. Together with the results of paired recordings, these experiments also suggest that the HVC_{RA}–interneuron excitatory coupling is sufficiently robust to enable single HVC_{RA} neurons to drive disynaptic, feedforward inhibition in HVC_X neurons.

HVC_{RA}–HVC_{INT} pairs

Paired recordings provided direct evidence of the excitatory nature of the synaptic contacts that HVC_{RA} axon collaterals make onto HVC_{INT}, consistent with the disynaptic model of feedforward inhibition between HVC_{RA} and HVC_X cells (Fig. 4*A*). A total of 13 HVC_{RA}–HVC_{INT} cell pairs revealed evidence of unidirectional or bidirectional synaptic coupling. Seven cases of HVC_{RA}-to-HVC_{INT} coupling were observed, and in six of those cases, DC-evoked action potentials in the HVC_{RA} neuron evoked a fast dPSP in the corre-

sponding HVC_{INT} (six of seven HVC_{RA} neurons evoked positive STAs in the interneuron; one of seven HVC_{RA} neurons evoked an IPSP). These dPSPs were characterized by a rapid time course and often by their large amplitudes (Fig. 4*B*, Table 2) (average peak amplitude, 2.0 ± 0.4 mV; average time to peak, 4.7 ± 0.5 ms; 25% rise time, 1.4 ± 0.1 ms; $n = 6$). The strength and excitatory nature of this connection was reflected in the observation that a single spike in the HVC_{RA} neuron often was sufficient to drive the interneuron to spike threshold (Fig. 4*A,C*) (five of six HVC_{RA}–HVC_{INT} pairs displayed such one-for-one spike coupling). This one-to-one spike coupling could account for how a single action potential in an HVC_{RA} neuron can evoke an IPSP in an HVC_X neuron. Furthermore, we noted that spike doublets or triplets in the HVC_{RA} neuron could trigger facilitation of EPSPs in the HVC_{INT} (Fig. 4*C*) ($n = 2$ pairs). On average, PSPs corresponding to doublet or triplet spikes were facilitated by 46% (paired *t* test; $p < 0.01$), measured at an average inter-PSP interval of 27 ms. Such facilitation may explain the observation that spike doublets in HVC_{RA} neurons sometimes were required to trigger IPSPs in HVC_X cells. In summary, HVC_{RA} neurons provide short-latency excitatory synaptic input to interneurons.

Paired recordings also revealed that interneurons could make synaptic contacts on HVC_{RA} neurons. Eight of the 13 coupled HVC_{RA}–HVC_{INT} pairs showed evidence of synaptic transmission from the interneuron to the PN. In six pairs, the interneuron action potential evoked an IPSP in the HVC_{RA} neuron (individual data not shown; average peak amplitude, −0.9 ± 0.2 mV; average time to peak, 10.7 ± 2.3 ms; 25% rise time, 1.7 ± 1.0 ms; $n = 6$) (for mean data, see Table 2), whereas in two pairs, the interneuron action potential evoked a dPSP in the HVC_{RA} cell (data not shown). The mean 25% rise time and the mean time to peak of these interneuron-evoked IPSPs were not significantly longer than those recorded in HVC_{INT}–HVC_X pairs, consistent with the idea that they were attributable to monosynaptic connections (for statistical comparisons, see Table 2). These results indicate that the HVC_{RA}–HVC_{INT} coupling is robust and bidirectional, at least at the population level. Notably, reciprocal connections were detected in two HVC_{RA}–HVC_{INT} pairs (data not shown). In both cases, the interneuron to PN interaction was inhibitory, whereas the PN to interneuron coupling was excitatory in one case and inhibitory in the other. The latter case may reflect a disynaptic pathway, because the PN–interneuron STA was of longer latency than the interneuron–PN STA (data not shown). The strong excitatory coupling from HVC_{RA} to HVC_{INT}

**Table 2. Characteristics of synaptic responses in connected HVC neuron pairs**

Pair type (number of pairs with given PSP/ total number of connected pairs of given type)	Peak amplitude (mV)	Time to peak (ms)	25% rise time (ms)
IPSPs			
$HVC_{RA} > HVC_X$ (25 of 29)	−1.5 ± 0.3	15.7 ± 1.0	4.8 ± 0.4
$HVC_X > HVC_{RA}$ (3 of 29)	−1.1 ± 0.1	9.9 ± 1.3	2.6 ± 0.7
$HVC_X > HVC_X$ (11 of 11)	−2.0 ± 0.4	15.4 ± 2.7	5.0 ± 1.7
$HVC_{INT} > HVC_X$ (19 of 20)	−1.2 ± 0.2	10.2 ± 0.9[a]	1.4 ± 0.3[b]
$HVC_{INT} > HVC_{RA}$ (6 of 13)	−0.9 ± 0.2	10.7 ± 2.3[c]	1.7 ± 1.0[c]
dPSPs			
$HVC_{RA} > HVC_{INT}$ (6 of 13)	2.0 ± 0.4	4.7 ± 0.5	1.4 ± 0.1
$HVC_X > HVC_{INT}$ (5 of 20)	1.2 ± 0.3	4.3 ± 0.4[d]	1.0 ± 0.6[d]
$HVC_{RA} > HVC_{RA}$ (4 of 4)	2.2 ± 1.1	9.1 ± 2.3	4.0 ± 0.3
$HVC_X > HVC_{RA}$ (4 of 29)	0.5 ± 0.1	8.3 ± 0.9	3.2 ± 0.3

[a]$p < 0.05$ versus $HVC_{RA} > HVC_X$, by ANOVA.
[b]$p < 0.05$ versus $HVC_{RA} > HVC_X$ and $HVC_X > HVC_X$, by ANOVA.
[c]$p > 0.05$ versus $HVC_{INT} > HVC_X$, by ANOVA.
[d]$p > 0.05$ versus $HVC_{RA} > HVC_{INT}$, by unpaired *t* test.
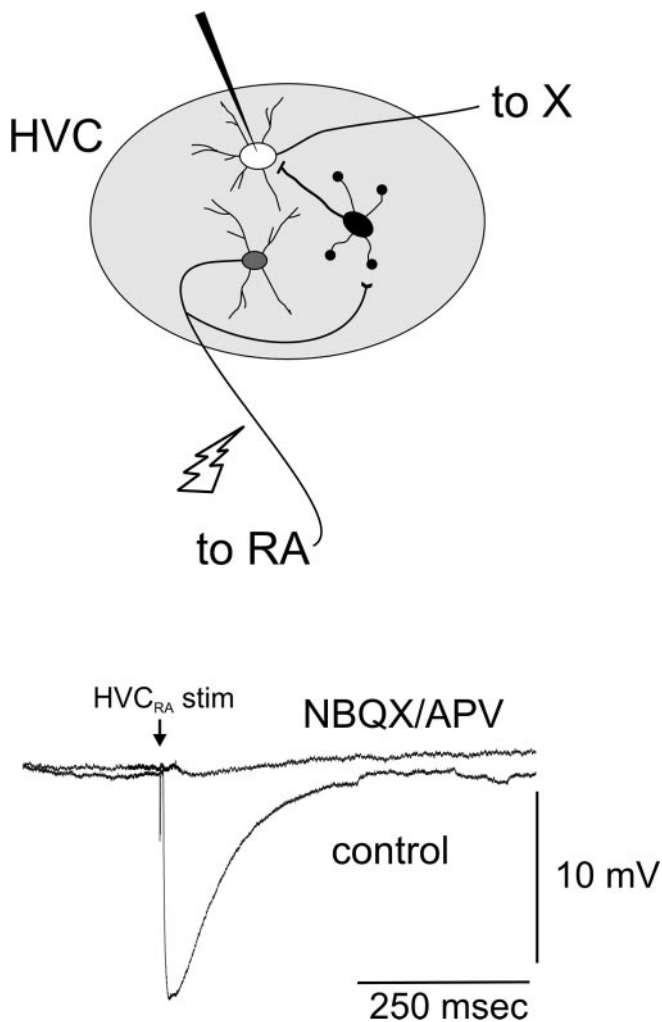
Figure 3. Antidromic stimulation of HVC$_{RA}$ axons can be used to characterize the pharmacological nature of the inhibitory interactions between HVC$_{RA}$ and HVC$_X$ cells. A schematic of the slice preparation (top), showing how antidromic stimulation of the HVC$_{RA}$ axon fiber bundle (lightning bolt) can be used to activate the HVC microcircuit while recording intracellularly from HVC$_X$ cells. In this model, local collaterals of the HVC$_{RA}$ axon excite HVC$_{INT}$, which ultimately drive IPSPs in the HVC$_X$ cell. Consistent with this idea, electrical stimulation of the HVC$_{RA}$ fibers drives IPSPs in HVC$_X$ cells (bottom; control), which are blocked by the bath application of ionotropic glutamate receptor antagonists (NBQX/APV).

and the existence of reciprocal inhibitory connections from HVC$_{INT}$ to HVC$_{RA}$ suggests that action potential activity in HVC$_{RA}$ neurons could be shaped by inhibitory feedback acting on a spike-by-spike basis.

HVC$_{INT}$–HVC$_X$ pairs
Paired recordings also revealed that interneurons could provide inhibitory input to HVC$_X$ cells. In almost all synaptically connected HVC$_{INT}$–HVC$_X$ cell pairs, an action potential in the interneuron evoked an IPSP in the HVC$_X$ cell (Fig. 5A) (19 of 20 cases; average peak amplitude, -1.2 ± 0.2 mV; average time to peak, 10.2 ± 0.9 ms; 25% rise time, 1.4 ± 0.3 ms; $n = 19$) (Table 2). In one case, unidirectional coupling from the HVC$_X$ neuron to the interneuron, in the form of a dPSP, was observed (data not shown). We noted that interneuron-evoked IPSPs in HVC$_X$ cells had faster rise times and times to peak than did IPSPs recorded in HVC$_{RA}$–HVC$_X$ cell pairs, although IPSPs of either type otherwise had a similar overall shape and time course (Fig. 5B) (for statistical comparisons, see Table 2). The very short onset latency of
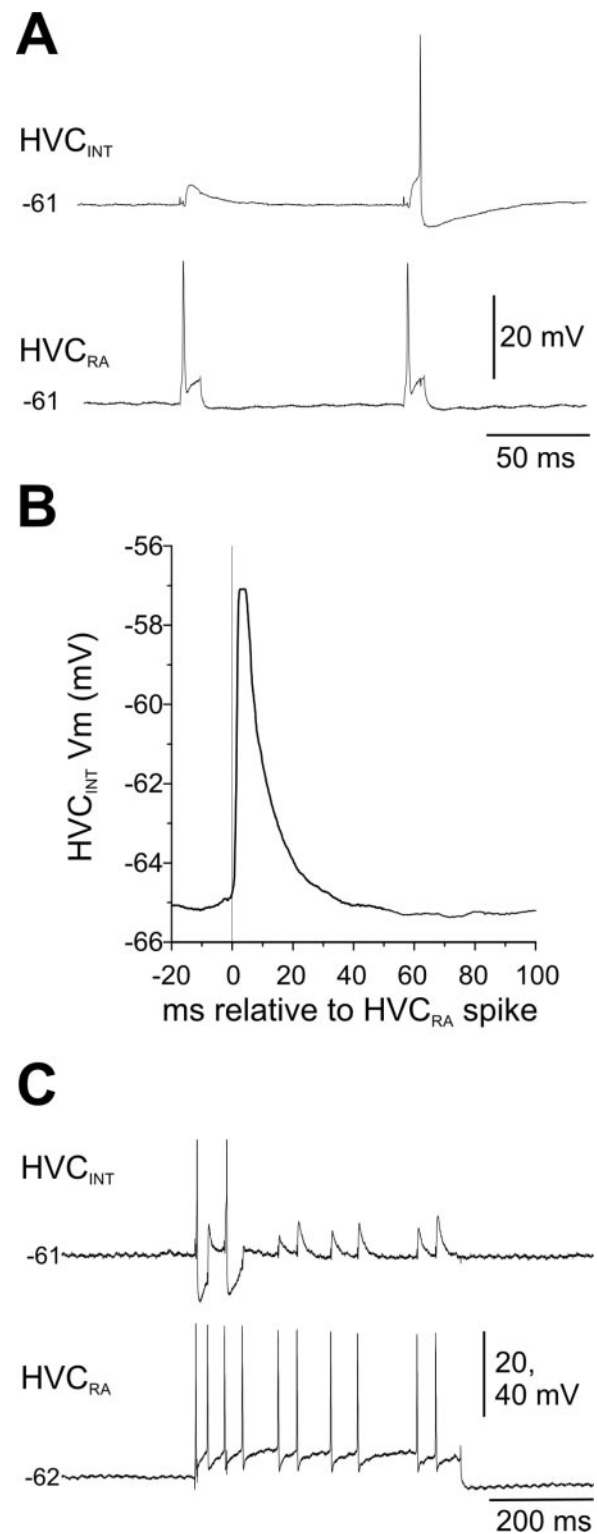
Figure 4. Dual intracellular recordings provide direct evidence of the excitatory synapses that HVC$_{RA}$ neurons make with HVC$_{INT}$. **A**, Depolarizing current pulses injected into the HVC$_{RA}$ neuron (bottom trace) elicit action potentials, which were followed at short latency by subthreshold (left) and suprathreshold (right) EPSPs in the HVC$_{INT}$. **B**, An STA of HVC$_{INT}$ membrane potential triggered off of the HVC$_{RA}$ action potential, from the cell pair shown in **A**. A fast-rising, short-latency-positive STA was detected after the HVC$_{RA}$ action potential, consistent with the idea that the HVC$_{RA}$ neuron makes an excitatory synapse with the interneuron. **C**, Longer depolarizing currents could evoke irregular spiking in the HVC$_{RA}$ neuron (bottom trace), which were paralleled by dEPSPs in the HVC$_{INT}$. In this case, note that the last six HVC$_{RA}$ spikes occurred in doublets and that the second dPSP was larger than the one immediately preceding it, suggestive of synaptic facilitation.

A

B

C

D
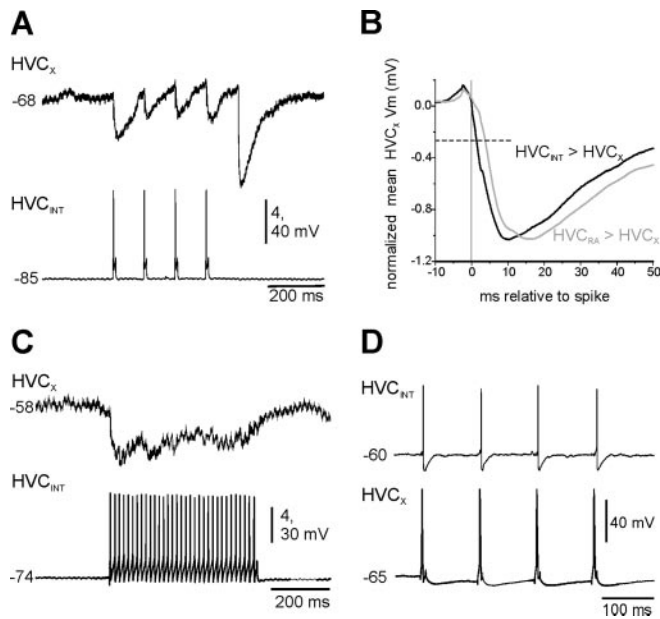
Figure 5. Dual intracellular recordings reveal that HVC_{INT} provide short-latency inhibition onto HVC_X cells. **A**, Raw membrane potential records from a synaptically coupled interneuron (bottom) and HVC_X cell (top). DC-evoked spikes could evoke robust IPSPs in the HVC_X cell; note that a spontaneous IPSP, presumably from another interneuron, occurred after the DC-evoked responses. **B**, The mean STA from all HVC_{INT}–HVC_X cell pairs compared with the mean STA from all HVC_{RA}–HVC_X cells pairs, showing the offset in the 25% rise times (horizontal dashed line) (see Table 2). The overall shapes of the STAs in the different cell pairs were very similar, but the HVC_{RA}–HVC_X STA was delayed relative to HVC_{INT}–HVC_X STA, suggesting that HVC_{RA} cells are connected indirectly with HVC_X cells. The STA conventions are as in Figures 2 and 4. **C**, Higher-frequency firing in an HVC_{INT} can drive a sustained hyperpolarization in the HVC_X cell. **D**, HVC_X cells in some cases could drive EPSPs in an HVC_{INT} cell. DC-evoked firing in the HVC_X cell (bottom trace) reliably evoked suprathreshold EPSPs in the HVC_{INT} (top trace). The HVC_{INT} also evoked IPSPs in the HVC_X cell (shown in Fig. 9D), indicating that interneurons and HVC_X cells can form reciprocal synaptic connections.

these responses (i.e., <1.4 ms) supports the view that the fast-spiking interneurons we recorded from here provide monosynaptic inhibitory input to HVC_X cells and thus are plausible cellular intermediaries through which HVC_{RA} neurons drive IPSPs in HVC_X cells. Another feature we noted was that longer action potential trains in the interneuron generated a sustained hyperpolarization in the HVC_X neuron, reminiscent of song-evoked hyperpolarizations that have been described in HVC_X cells from *in vivo* recordings (Fig. 5C) (n = 9 cases). Therefore, interneurons evoke short-latency IPSPs in HVC_X cells and are likely to constitute the distal arm of the disynaptic pathway linking HVC_{RA} to HVC_X cells.

Paired recordings also provided evidence of reciprocal connectivity between interneurons and HVC_X cells (Figs. 5D) (see Fig. 9D, right) (n = 4 pairs). In all four reciprocally connected pairs, the HVC_X neuron action potential evoked a dPSP in the interneuron; in two pairs, these PSPs were demonstrably excitatory (Fig. 5D, Table 2) (average peak amplitude, 1.2 ± 0.3 mV; average time to peak, 4.3 ± 0.4 ms; 25% rise time, 1.0 ± 0.6 ms). The rapid onset and time to peak of the dPSPs were similar to those recorded in HVC_{RA}–HVC_{INT} cell pairs (for statistical comparisons, see Table 2). In all of our reciprocally connected HVC_{INT}–HVC_X cell pairs, the interneuron action potential evoked an IPSP in the HVC_X neuron. Therefore, HVC_X neurons can form strong excitatory synapses onto interneurons that provide them with reciprocal inhibitory input, suggesting that action

potential activity in HVC_X neurons, as with HVC_{RA} neurons, could be shaped on a spike-by-spike basis by inhibitory feedback.

Pharmacology of HVC_{INT}-mediated inhibition

Previous studies showed that IPSPs in HVC neurons are mediated by several different neurotransmitter receptors, including ionotropic $GABA_A$ receptors and metabotropic GABA and glutamate receptors (Schmidt and Perkel, 1998; Dutar et al., 1999, 2000; Rosen and Mooney, 2003). The relatively fast onset and time to peak of the IPSPs we recorded in HVC_{INT}–HVC_X cell pairs suggested that ionotropic $GABA_A$ receptors, and not metabotropic receptors, were involved. We tested this idea in several ways. First, we bath applied PTX (50 μM), a $GABA_A$ receptor blocker, while recording from synaptically coupled pairs of cells. In two HVC_{INT}–HVC_X pairs and one HVC_{RA}–HVC_X cell pair, spike-evoked IPSPs in the HVC_X cell were abolished by this treatment, indicating that in both types of connections, ionotropic $GABA_A$ receptors mediated the IPSP (Fig. 6A,B) (control, −1.2 ± 0.2 mV; PTX, 0.0 ± 0.1 mV; n = 3; p < 0.05; ANOVA). Second, we evoked fast, short-latency IPSPs in HVC_X cells by antidromically stimulating HVC_{RA} neurons and then bath applied PTX (50 μM). Treatment with PTX consistently and completely abolished the electrically evoked short-latency IPSP and unmasked a short-latency dPSP (Fig. 7A, inset) (n = 12 cases; control, −13.7 ± 0.6 mV; PTX, +4.9 ± 0.3 mV; p = 0.000012). Third, paired recording revealed that interneuron-evoked IPSPs in an HVC_X cell were unaffected by ionotropic glutamate receptor blockers (Fig. 6C), although EPSPs in the interneuron and IPSPs in the HVC_X cell evoked by antidromic stimulation of HVC_{RA} neurons were blocked by this treatment (Fig. 6D) (n = 1). These experiments show that $GABA_A$ receptors mediate the fast IPSPs evoked in HVC_X cells by both interneurons and HVC_{RA} cells. These experiments also reveal monosynaptic and/or polysynaptic excitatory pathways from HVC_{RA} to HVC_X cells, which are normally suppressed or otherwise masked by $GABA_A$-mediated inhibition.

Prolonged blockade of $GABA_A$ receptors in HVC also unmasked more complex synaptic interactions between HVC_{RA} and HVC_X cells. Notably, after 15–20 min of PTX application, antidromic stimulation of HVC_{RA} neurons evoked larger EPSPs capable of eliciting a high-frequency action potential burst in the HVC_X neuron (Fig. 6E, middle). In several cells (n = 3), repetitive bursting followed a single antidromic stimulus (Fig. 7A). PTX treatment also unmasked evidence for slow inhibitory signaling from HVC_{RA} to HVC_X cells. In two cells, a prolonged, multiphasic response was evoked by HVC_{RA} stimulation shortly after applying PTX but before the emergence of the dPSP (Fig. 7B, left). In addition, prolonged hyperpolarizations sometimes followed the shorter-latency dEPSPs (Fig. 7A,B, right). The shorter-latency EPSPs, as well as associated prolonged hyperpolarizations, were completely abolished by a combination of NBQX and D-APV, indicating they were mediated in part via monosynaptic and/or polysynaptic pathways involving ionotropic glutamate receptors (Figs. 6E, right; 7A) (n = 9 cases; PTX, +8.8 ± 1.7 mV; NBQX/D-APV, −0.1 ± 0.12 mV; p < 0.001; Mann–Whitney U test). In summary, these pharmacological experiments show that fast-spiking interneurons evoke IPSPs in HVC_X cells via $GABA_A$ receptors. Furthermore, HVC_{RA} neurons drive excitatory and inhibitory responses in HVC_X neurons via synaptic pathways that involve ionotropic glutamate receptors.
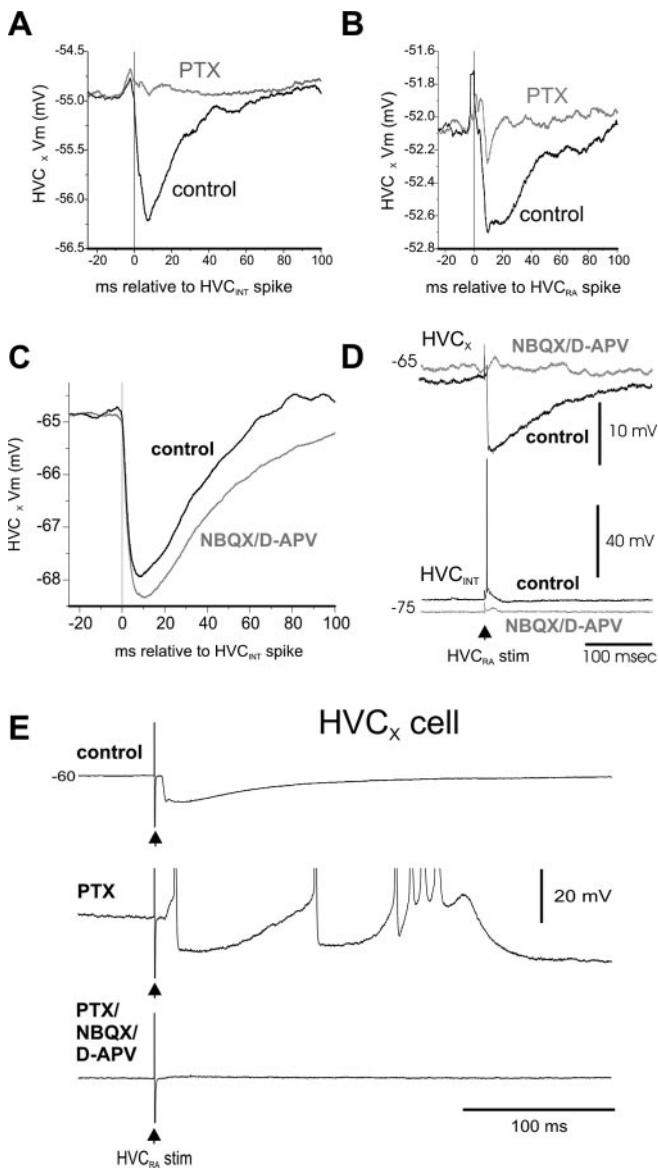
Figure 6. The IPSPs evoked in HVC$_X$ cells by both interneurons and HVC$_{RA}$ cells were mediated by GABA$_A$ receptors. **A**, In this interneuron–HVC$_X$ cell pair, action potentials in the interneuron evoked a hyperpolarizing response in the HVC$_X$ cell, indicative of an IPSP (control). Bath application of the GABA$_A$ receptor antagonist PTX blocked the IPSP. **B**, A negative STA of the HVC$_X$ membrane potential evoked by action potentials in an HVC$_{RA}$ neuron was also blocked by the bath application of PTX. **C**, An IPSP evoked in an HVC$_X$ cell by DC-evoked action potentials in a simultaneously recorded interneuron did not decrement in the presence of ionotropic glutamate receptor blockers NBQX and D-APV. **D**, In the same pair of neurons, antidromic stimulation of the HVC$_{RA}$ fiber tract (arrow) evoked an EPSP in the interneuron (bottom; control) and an IPSP in the simultaneously recorded HVC$_X$ cell (top; control). Subsequent bath application of NBQX/ D-APV greatly reduced the excitation onto the interneuron and abolished the IPSP in the HVC$_X$ cell. Thus, in the presence of compounds that block fast excitatory transmission, inhibition from HVC$_{RA}$ onto HVC$_X$ cells is abolished, although inhibition from the interneuron onto the HVC$_X$ cell persists. **E**, Antidromic stimulation of the HVC$_{RA}$ fiber tract was used to evoke an IPSP in an HVC$_X$ cell (control). Subsequent bath application of PTX abolished the IPSP, unmasking robust EPSPs, resulting in repetitive action potential discharge in the HVC$_X$ neuron (PTX; middle; 4 spikes in burst; mean burst rate, 111 Hz). The subsequent addition of the ionotropic glutamate receptor blockers NBQX and D-APV blocked all synaptic responses in the HVC$_X$ cell.

Interneurons that evoke IPSPs are PV positive

The interneurons that evoke IPSPs in HVC$_X$ cells are fast-spiking cells with varicose dendrites (Fig. 1C,D). Previous immunohistochemical studies indicated that fast-spiking HVC interneurons
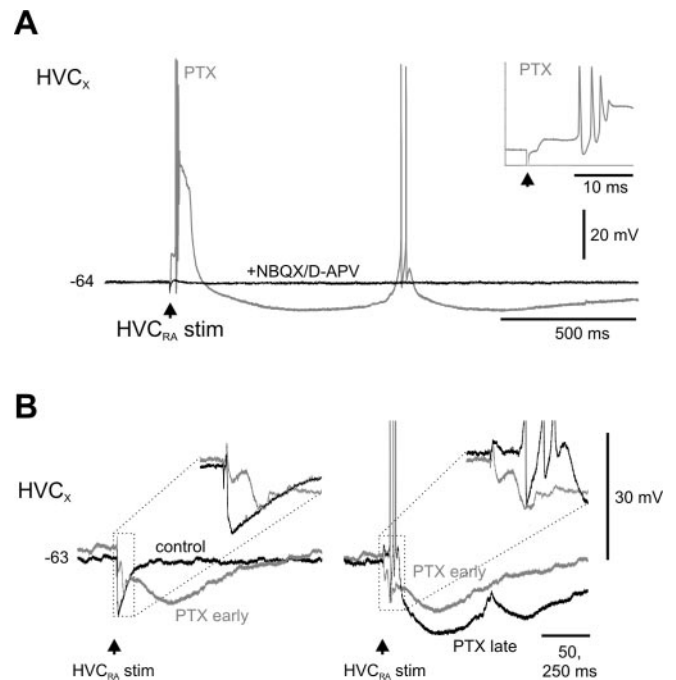
Figure 7. Blocking GABA$_A$-mediated inhibition in HVC could unmask additional excitatory and inhibitory synaptic pathways from HVC$_{RA}$ to HVC$_X$ neurons. **A**, In a PTX-treated brain slice, antidromic stimulation of HVC$_{RA}$ neurons could evoke repetitive bursting (early burst: 3 spikes, 200 Hz mean burst rate; later burst: 2 spikes, 59 Hz burst rate) and slow hyperpolarizing responses, which were blocked by the bath application of the ionotropic glutamate receptor antagonists NBQX and D-APV. **B**, Before PTX treatment, antidromic stimulation of the HVC$_{RA}$ fibers evoked a fast IPSP in an HVC$_X$ neuron (control); subsequent PTX treatment blocked the early, fast IPSP and unmasked a multiphasic IPSP that included a slow component (PTX early). At later times during the treatment (PTX late), the same stimulation evoked an initial excitatory response, followed by a prolonged, biphasic hyperpolarization. The subthreshold depolarization that occurs during the middle of the slow, biphasic hyperpolarization is believed to be similar to the event associated with the longer-latency bursting behavior in **A**.

with varicose dendrites are PV positive (PV+) (Wild et al., 2005) but did not resolve whether PV+ interneurons are a source of inhibitory input onto HVC PNs. We used anti-PV antibodies and intracellular staining with Neurobiotin to determine whether the interneurons that provided inhibitory input onto HVC$_X$ cells were PV+. In two HVC$_{INT}$–HVC$_X$ pairs, morphologically and physiologically identified fast-spiking interneurons that evoked IPSPs in HVC$_X$ cells were PV+, whereas the corresponding HVC$_X$ cells were PV negative (PV−) (Fig. 8A). We did note, however, that HVC$_X$ neurons were sometimes in extremely close apposition to PV+ cell bodies (Fig. 8B) (n = 2 cases). These results show that PV+ interneurons provide some of the inhibitory input onto HVC PNs that innervate basal ganglia structures in the songbird brain.

Homotypic synaptic interactions

Paired recordings also revealed synaptic interactions between neurons of the same type. Eleven HVC$_X$ pairs showed signs of unidirectional inhibitory synaptic coupling, all in the form of spike-evoked IPSPs (individual data not shown; average peak amplitude, −2.0 ± 0.4 mV; average time to peak, 15.4 ± 2.7 ms; 25% rise time, 5.0 ± 1.7 ms; n = 11) (for mean data, see Table 2). These IPSPs were presumably mediated by intervening interneurons, in part because recordings previously described indicated that HVC$_X$ neurons can make excitatory synapses onto HVC$_{INT}$. Furthermore, the mean 25% rise time of IPSPs evoked in HVC$_X$– HVC$_X$ cell pairs was significantly longer than that of IPSPs re-

corded in HVC$_{INT}$–HVC$_X$, but not HVC$_{RA}$–HVC$_X$, cell pairs (for statistical comparisons, see Table 2). Five HVC$_{RA}$ pairs were also recorded: four exhibited unidirectional dEPSPs (Table 2), whereas one showed an IPSP (data not shown). Finally, one synaptically coupled interneuron pair was detected that exhibited a unidirectional IPSP (data not shown) (Table 1). Therefore, inhibitory as well as excitatory connections serve to synaptically link homotypic as well as heterotypic pairs of neurons within HVC.

Divergent and convergent synaptic connections in HVC

The extensive local axonal network of both PNs and interneurons raises the possibility of divergent and convergent patterns of synaptic connectivity within HVC. We were able to detect both divergent and convergent synaptic connections by recording from one HVC neuron with a fixed electrode and moving a second electrode about the slice to sequentially record from a series of other cells that were either its presynaptic or postsynaptic partner. In four of these sequential paired recordings, the fixed electrode was in an interneuron, whereas the moveable electrode encountered a series of PNs. Three qualitative observations resulted from these recordings. First, a single interneuron can evoke IPSPs in both HVC$_{RA}$ and HVC$_X$ neurons (Fig. 9A). Second, a single interneuron can make divergent inhibitory synapses on several HVC$_X$ cells (Fig. 9B). Third, a single interneuron can receive convergent input from two or more HVC$_{RA}$ neurons (data not shown). In three other sequential paired recordings, the fixed electrode was placed in an HVC$_X$ neuron, whereas the moveable electrode recorded from HVC$_{INT}$ and/or HVC$_{RA}$ neurons. These recordings revealed that both HVC$_{INT}$ and HVC$_{RA}$ neurons can provide inhibitory input onto the same HVC$_X$ cell (Fig. 9C). Therefore, single interneurons can contact PNs of both types and can receive convergent excitatory input from HVC$_{RA}$ neurons.

Interneurons also receive convergent excitatory input from PNs of different types. We examined interactions between the three cell types by coupling antidromic stimulation of HVC$_{RA}$ neurons while using two electrodes to record from HVC$_{INT}$–HVC$_X$ cell pairs. In all six pairs, the HVC$_{INT}$ evoked IPSPs in the HVC$_X$ cell; in two of these pairs, the HVC$_X$ cell provided reciprocal excitation to the interneuron. In all of these pairs, antidromic activation of the HVC$_{RA}$ axon collateral network evoked an EPSP in the HVC$_{INT}$ cell and an IPSP in the HVC$_X$ cell (Fig. 9D). These results show that the two PN types provide convergent excitatory input onto single interneurons, which in turn provide an inhibitory link between the HVC PNs. The various features of the local synaptic organization of HVC revealed in this study are summarized in Figure 10.

Frequency of synaptic connections between different HVC cell types

We also performed additional paired recordings to provide an estimate both of the frequency of pair types that we encountered using these recording methods and the frequency of synaptic connections that we detected between neurons of given types. A
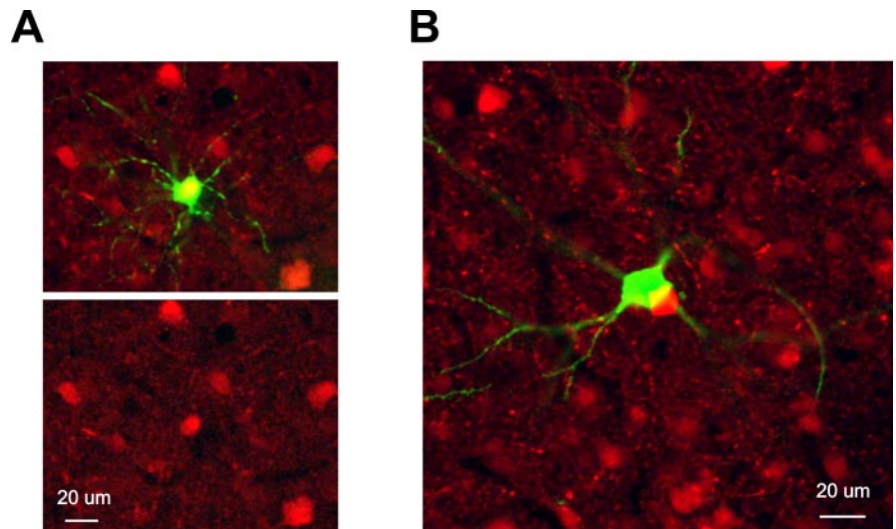
Figure 8. Fast-spiking interneurons that evoked IPSPs in HVC$_X$ neurons are PV +. **A**, Top, A single optical section of a confocal image of an intracellularly stained interneuron (green) with immunohistochemical staining for PV (red). Action potentials in this interneuron evoked IPSPs in an HVC$_X$ cell (data not shown). In the bottom panel, only the red wavelength is shown, showing that the soma of the interneuron was PV +. **B**, An HVC$_X$ neuron (green) that received inhibitory input from a fast-spiking interneuron; a PV + cell body was closely apposed to the HVC$_X$ neuron soma.

total of 96 pairs was obtained, 18 of which displayed either unidirectional or bidirectional synaptic coupling (~19%; note that the connected pairs from this sample contributed to the total pool of connected pairs represented in Table 2 and discussed in previous sections of Results) (Table 1). Several features of this sample are notable. First, the vast majority of pairs that we obtained [77 of 96 (~80%)] contained at least one HVC$_X$ neuron, likely reflecting the fact that these cells are relatively numerous and large, and typically afford the most stable recordings with the sharp electrode methods used in this study. Second, almost two-thirds [61 of 96 (63%)] of all pairs consisted of HVC$_{RA}$ neurons, which despite their small size are highly abundant (Kirn et al., 1991; Wild et al., 2005). Perhaps as a result of these various factors, HVC$_{RA}$–HVC$_X$ neuron pairs made up almost one-half this sample [46 of 96 (~48%)]. Finally, in contrast to our overall larger sample of HVC$_{RA}$ and HVC$_X$ neuron pairs, this smaller sample exhibited a higher proportion of HVC$_X$-to-HVC$_{RA}$ synaptic connections [5 of 6 (83%) vs 7 of 29 (24%)] and included three reciprocally connected cell pairs.

Discussion

The present study reveals several synaptic features likely to be important to the song-related motor and auditory functions of HVC. First, HVC$_{RA}$ neurons excite interneurons, which inhibit HVC$_X$ neurons, providing a feedforward inhibitory mechanism linking song premotor and basal ganglia projecting pathways emanating from HVC. This feedforward inhibition could help shape motor-related activity transmitted to the AFP and generate cell type-specific patterns of auditory activity. Second, interneurons innervate multiple PNs of both types and thus could coordinate their activity. Finally, HVC contains reciprocally connected PNs and interneurons, similar to other pattern-generating networks.

Feedforward inhibition and excitation from HVC$_{RA}$ to HVC$_X$ neurons

These studies show that HVC$_X$ cells, which innervate basal ganglia structures important to vocal plasticity (Nottebohm et al., 1976, 1982; Bottjer et al., 1984; Scharff and Nottebohm, 1991),
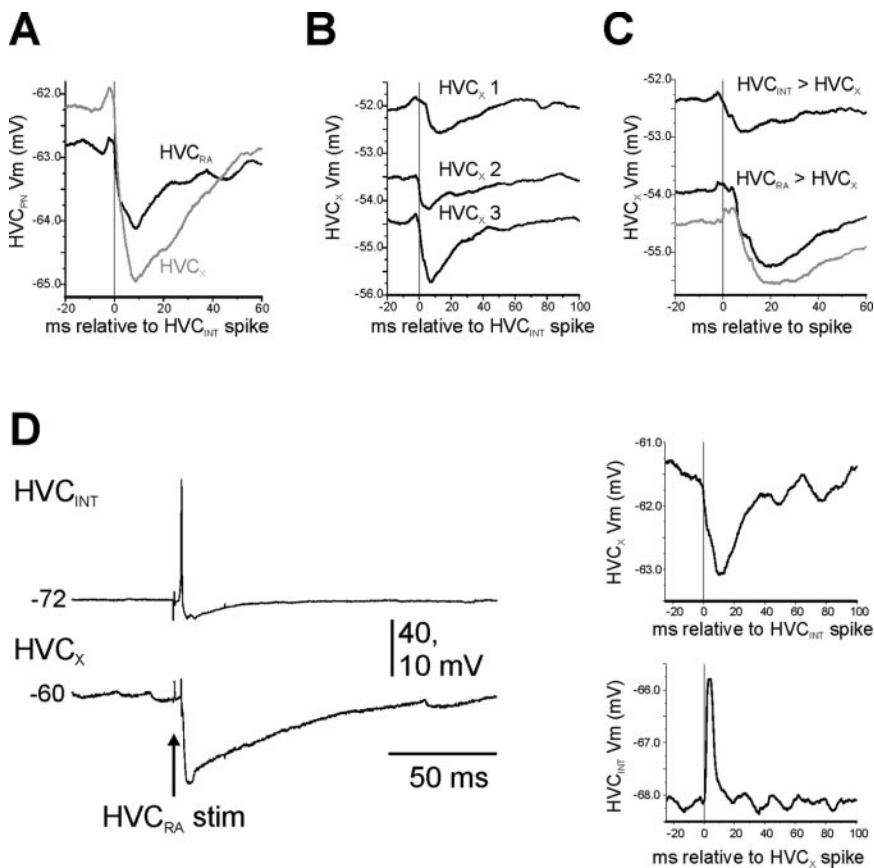
Figure 9. Sequential paired recordings reveal divergent and convergent inhibitory and excitatory synaptic connections in HVC. *A*, Sequential recordings from an HVC_{RA} and HVC_X neuron while maintaining an intracellular recording from an interneuron. The averages of both PN membrane potentials triggered off of the action potentials of the interneuron showed that a single interneuron could evoke IPSPs in both cells. *B*, Sequential recordings from three different HVC_X neurons (HVC_X 1–3) show that action potentials in a single interneuron could evoke IPSPs in all three HVC_X cells. *C*, Sequential recordings from an interneuron and two different HVC_{RA} neurons while maintaining a recording from a single HVC_X cell show that both HVC_{RA} cells and the interneuron can provide inhibitory input onto the same HVC_X cell. *D*, A reciprocally connected interneuron–HVC_X cell pair also receives synaptic input from HVC_{RA} axon collaterals. Antidromic stimulation of HVC_{RA} axons evokes an EPSP in the interneuron (top) and an IPSP in the HVC_X cell (bottom). Spike-triggered averaging reveals that the interneuron evokes an IPSP in the HVC_X cell, which in turn could evoke a dPSP in the interneuron. This is the same HVC_X–interneuron pair shown in Figure 5*D*, in which action potentials in the HVC_X cell evoked suprathreshold EPSPs in the interneuron. These recordings show that both HVC_X and HVC_{RA} axon collaterals can excite the same interneuron in HVC.

are inhibited directly by interneurons and indirectly by HVC PNs of both types. The IPSPs from HVC_{RA} to HVC_X cells were most likely mediated via disynaptic, feedforward mechanisms, because: (1) antagonists of ionotropic glutamate receptors blocked all inhibitory synaptic transmission in HVC_X cells evoked by antidromic stimulation of HVC_{RA} fibers; (2) in paired recordings, $GABA_A$ receptor blockers abolished IPSPs evoked in HVC_X cells by either HVC_{INT} or HVC_{RA}; (3) HVC_{RA} neurons drive fast rise-time EPSPs mediated by ionotropic glutamate receptors on HVC_{INT} and on their extrinsic targets in the nucleus RA; (4) interneurons drive IPSPs in HVC_X cells with faster rise times than IPSPs driven in HVC_X cells by HVC_{RA} neurons; and (5) spike doublets in HVC_{RA} cells could evoke excitatory synaptic facilitation in interneurons and were sometimes required to trigger IPSPs in HVC_X cells. Similar disynaptic mechanisms likely underlie IPSPs detected in pairs of HVC_X cells, because the rise times of these IPSPs were relatively slow, like those in HVC_{RA}–HVC_X cell pairs, and because HVC_X cells evoke EPSPs in interneurons. Additionally, monosynaptic and polysynaptic excitatory pathways and polysynaptic inhibitory pathways link HVC_{RA} to HVC_X cells but are normally masked by fast inhibition.

Reciprocal connections between HVC PNs and interneurons

Although a common pattern of synaptic flow was from HVC_{RA} to HVC_X cells, HVC_X neurons also could evoke depolarizing or hyperpolarizing responses in some HVC_{RA} neurons, and reciprocally coupled heterotypic PN pairs were sometimes encountered. Consistent with the idea that HVC_{RA} and HVC_X cells are bidirectionally connected via interneurons, single interneurons could be excited by PNs of both types and also could inhibit multiple PNs of both types. Reciprocal inhibitory interactions between the two PN types may have important implications for the functioning of the HVC in response to song playback and during singing. HVC_{RA} and HVC_X cells alternate in their firing during playback of the BOS (Mooney, 2000), which could be explained if these two types of excitatory neurons were coupled via reciprocal inhibition. More generally, half-center oscillators, wherein two neurons make reciprocally inhibitory connections, can produce highly rhythmic bursts of action potential activity (Cropper and Weiss, 1996; Marder and Bucher, 2001; Cymbalyuk et al., 2002). Although some HVC_{RA} and HVC_X neurons form architecture characteristic of half-center oscillators, the importance of such an arrangement for generating rhythmical activity underlying singing is unclear, because adult song structure remains intact immediately after selective ablation of HVC_X neurons (Scharff et al., 2000). Therefore, other mechanisms in HVC can generate or transmit patterned song premotor activity when HVC_X neurons are reduced or absent. One generative mechanism could be reciprocal coupling between excitatory HVC_{RA} neurons and fast-spiking inhibitory interneurons. Indeed, reciprocally connected excitatory and inhibitory neurons can form bistable networks, generating either no output or low-frequency rhythms, depending on the amount of excitatory drive applied to the excitatory cells (Borgers and Kopell, 2005).

Functional implications of divergent and convergent synaptic connections

Sequential paired recordings revealed that interneurons divergently innervate PNs of both types, an arrangement that could synchronize the firing of multiple HVC cells, as occurs in sleeping birds (Rauske et al., 2003). Although synaptically coupled cell pairs recorded here were typically in close proximity (cf. Feldmeyer et al., 1999), intracellular staining showed that interneuron processes are extensive (Fig. 1*C*) (Katz and Gurney, 1981; Mooney, 2000; Wild et al., 2005), raising the possibility of a more widespread influence on HVC synchrony. Although none of the paired recordings we obtained displayed evidence of electrotonic coupling, gap junctions have been detected in HVC (Gahr and Garcia-Segura, 1996), affording a potential synchronizing influ-
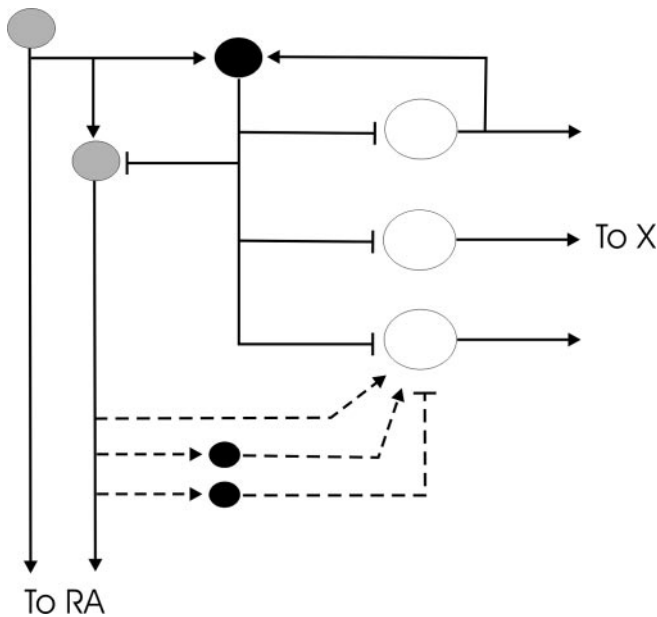
Figure 10. The major synaptic features of the HVC microcircuit revealed in the present study by paired recordings and antidromic stimulation of HVC_{RA} neurons are shown. HVC_{RA} (gray circles) and HVC_X (white circles) neurons form excitatory synaptic connections (arrows) on interneurons (black circles), which provide divergent inhibitory input (t-endings) on PNs of both types. Fast excitation is mediated by ionotropic glutamate receptors, whereas fast inhibition is mediated by $GABA_A$ receptors. Additional polysynaptic and possibly monosynaptic excitatory pathways and polysynaptic inhibitory pathways also provide a synaptic linkage from HVC_{RA} to HVC_X neurons (dashed lines). These monosynaptic and polysynaptic pathways are dependent on ionotropic glutamate receptors, presumably involving direct synapses between HVC_{RA} axon collaterals and HVC_X neurons and intervening synapses between HVC_{RA} axon collaterals and other HVC interneurons.

ence on HVC activity in addition to or in conjunction with the interneuron network (Deans et al., 2001; Galarreta and Hestrin, 2002; Long et al., 2004). Divergent patterns of interneuron-mediated inhibition have also been invoked to explain HVC_{RA} neuronal activity during singing, which is characterized by temporally sparse action potential bursts thought to propagate sequentially through an array of these neurons (Hahnloser et al., 2002). Convergent excitatory input from HVC_{RA} neurons onto interneurons, coupled with divergent projections from single interneurons onto multiple HVC_{RA} neurons, could form a synaptic substrate for sequence propagation throughout the HVC_{RA} neuronal array. An important future goal will be to determine whether single interneurons synapse on multiple HVC_{RA} neurons, as shown here for HVC_X neurons. Furthermore, reciprocal connectivity between single PNs of either type and interneurons, as seen here, could generate negative feedback, limiting spike burst duration and augmenting the temporal sparseness that characterizes HVC PN activity during singing and song playback (Mooney, 2000; Hahnloser et al., 2002). Indeed, simply adding the mean time to peak of HVC_{RA} to interneuron and interneuron to HVC_{RA} PSPs yields a value of ~15 ms (Table 2). This value is similar to the spike burst duration of HVC_{RA} neurons during singing (typically ~6 ms *in vivo*) (Hahnloser et al., 2002) and could be regarded as an estimate of the mean upper limit for the time scale over which reciprocal interactions between HVC_{RA} and interneurons might occur.

Types of interneuron-mediated inhibition
Previous *in vivo* and *in vitro* studies showed that HVC_X neurons receive remarkably diverse forms of inhibition, including fast

IPSPs mediated by $GABA_A$ receptors and slow IPSPs mediated by $GABA_B$ and metabotropic glutamate receptors (Schmidt and Perkel, 1998; Dutar et al., 1999, 2000; Hahnloser et al., 2002; Rosen and Mooney, 2003). This functional diversity may be reflected in part by the diverse calcium-binding protein expression patterns of HVC interneurons, which contain various combinations of PV, calbindin, and calretinin (Wild et al., 2005). The present study shows that at least some fast-spiking interneurons are PV+ and evoke $GABA_A$ receptor-mediated IPSPs in HVC_X cells. This result links previous observations that fast-spiking interneurons are PV+ (Wild et al., 2005) and that PV+ cells coexpress the synthetic enzyme for GABA (Zuschratter et al., 1987). Because PV+ neurons evoke fast, $GABA_A$-mediated IPSPs in HVC_X cells, they functionally resemble PV+ interneurons in the mammalian cortex, which evoke fast $GABA_A$-mediated inhibitory synaptic currents in pyramidal neurons (Maccaferri et al., 2000). Interneurons also are the likely source of the slow IPSPs evoked in HVC_X cells by antidromically stimulating HVC_{RA} neurons in the presence of PTX. These slow IPSPs could be blocked by antagonists of ionotropic glutamate receptors, suggesting they arise polysynaptically through HVC interneurons, rather than monosynaptically via HVC_{RA} axon collaterals (i.e., via metabotropic glutamate receptors) (Schmidt and Perkel, 1998; Dutar et al., 1999, 2000). An important future goal will be to further characterize the correspondence between morphological, biochemical and functional properties of different HVC interneuron types.

Relevance to the auditory and motor properties of HVC
The inhibitory and excitatory linkage from HVC_{RA} to HVC_X cells could have important consequences for the processing of auditory and song motor activity in HVC. Exquisite auditory selectivity for the BOS is a hallmark of HVC neuronal responses in anesthetized songbirds (Margoliash, 1983; Theunissen and Doupe, 1998), and the HVC local circuit is thought to play a role in shaping this selectivity (Lewicki and Konishi, 1995; Lewicki and Arthur, 1996; Mooney, 2000; Rosen and Mooney, 2003; Coleman and Mooney, 2004). Intracellular recordings from urethane anesthetized zebra finches have shown that BOS playback evokes distinct subthreshold responses in the two HVC PNs, including sustained and mostly subthreshold depolarization in HVC_{RA} neurons and prolonged hyperpolarizing responses punctuated by phasic excitation in HVC_X cells (Mooney, 2000). These hyperpolarizing responses help shape the pattern of BOS-evoked firing in HVC_X cells and likely arise through local inhibition onto HVC_X cells (Rosen and Mooney, 2003). Indeed, inactivating HVC by local application of GABA unmasks prolonged BOS-evoked depolarizations in HVC_X cells, pointing to a local source of inhibition (M. Rosen and R. Mooney, unpublished observations). Furthermore, BOS-evoked hyperpolarizations in HVC_X cells closely correlate with firing in interneurons (Mooney, 2000), and these interneurons appear to be the same type shown here that drive fast IPSPs in HVC_X cells, because both cells are fast spiking, have varicose dendrites, and are PV+ (Mooney, unpublished observations). However, BOS-evoked hyperpolarizations in HVC_X cells involve slow G-protein-mediated potassium currents, with only a cryptic contribution from chloride-mediated currents typical of ionotropic $GABA_A$ receptors (Rosen and Mooney, 2003). Therefore, additional inhibitory pathways normally quiescent in the *in vitro* preparation must be active during song playback, possibly including the slow inhibitory pathways unmasked by PTX that indirectly link HVC_{RA} to HVC_X cells.

Chronic recordings in singing birds reveal that activity in the AFP is closely locked to the acoustical features of the bird's song

and persists after deafening, suggesting a motor origin (Hessler and Doupe, 1999; Leonardo, 2002). The inhibitory and excitatory synaptic linkage from HVC_{RA} to HVC_X cells seen here suggests mechanisms by which HVC circuitry could shape and convey song motor activity to the AFP. First, monosynaptic excitation and lagging disynaptic inhibition from HVC_{RA} cells could generate tightly correlated phasic excitation in HVC_X cells (Pouille and Scanziani, 2001), which may enhance signal propagation in the AFP. Second, inhibition can synchronize neuronal firing (Lytton and Sejnowski, 1991; Bush and Sejnowski, 1996) and, in HVC_X cells, may also trigger burst firing by deinactivation of low-threshold calcium channels (Kubota and Saito, 1991; Rosen and Mooney, 2003), two features that could facilitate transmission of excitatory signals to the AFP. Third, by analogy to mammalian basal ganglia circuitry (Afifi, 1994; Wichmann and DeLong, 1996; Reiner, 2002), motor-driven inhibition from HVC_{RA} onto HVC_X cells could disinhibit downstream targets in the AFP (Wilson, 1993; Sil'kis, 2002; Nambu, 2004). Indeed, inhibitory synapses in the AFP [i.e., between Area X and the medial nucleus of the dorsolateral thalamus (Luo and Perkel, 2002)] could effect the necessary sign inversion for such disinhibition. Fourth, high-frequency (>100 Hz) firing in the HVC_{RA} neuron sometimes was required to evoke an IPSP in the HVC_X cell, apparently because of facilitation at the HVC_{RA}–interneuron synapse. Given the propensity for HVC_{RA} neurons to fire in high-frequency bursts during singing (Hahnloser et al., 2002), such facilitation could be integral to shaping premotor activity in HVC_X neurons and thus modulating AFP song motor activity. Finally, we noted that antidromic stimulation of HVC_{RA} neurons evoked an IPSP that was nearly 10-fold greater in amplitude than unitary IPSPs evoked in HVC_X neurons by either interneurons or HVC_{RA} cells, suggesting that multiple interneurons converge directly onto single HVC_X cells and that multiple HVC_{RA} neurons converge indirectly onto HVC_X cells. This pattern of convergence in HVC may enable the activity of a larger ensemble of HVC_{RA} neurons to be integrated in single cells projecting to the AFP. Because HVC_{RA} neurons fire in a temporally sparse manner during singing and song playback (Mooney, 2000; Hahnloser et al., 2002), such synaptic integration may facilitate larger time scale representations of song in the AFP.

References

Afifi AK (1994) Basal ganglia: functional anatomy and physiology. Part 1. J Child Neurol 9:249–260.

Borgers C, Kopell N (2005) Effects of noisy drive on rhythms in networks of excitatory and inhibitory neurons. Neural Comput, in press.

Bottjer SW, Miesner EA, Arnold AP (1984) Forebrain lesions disrupt development but not maintenance of song in passerine birds. Science 224:901–903.

Brainard MS, Doupe AJ (2000) Interruption of a basal ganglia-forebrain circuit prevents plasticity of learned vocalizations. Nature 404:762–766.

Bush P, Sejnowski T (1996) Inhibition synchronizes sparsely connected cortical neurons within and between columns in realistic network models. J Comput Neurosci 3:91–110.

Coleman MJ, Mooney R (2004) Synaptic transformations underlying highly selective auditory representations of learned birdsong. J Neurosci 24:9251–9265.

Cropper EC, Weiss KR (1996) Synaptic mechanisms in invertebrate pattern generation. Curr Opin Neurobiol 6:833–841.

Cymbalyuk GS, Gaudry Q, Masino MA, Calabrese RL (2002) Bursting in leech heart interneurons: cell-autonomous and network-based mechanisms. J Neurosci 22:10580–10592.

Deans MR, Gibson JR, Sellitto C, Connors BW, Paul DL (2001) Synchronous activity of inhibitory networks in neocortex requires electrical synapses containing connexin36. Neuron 31:477–485.

Dutar P, Vu HM, Perkel DJ (1998) Multiple cell types distinguished by physiological, pharmacological, and anatomic properties in nucleus HVc of the adult zebra finch. J Neurophysiol 80:1828–1838.

Dutar P, Vu HM, Perkel DJ (1999) Pharmacological characterization of an unusual mGluR-evoked neuronal hyperpolarization mediated by activation of GIRK channels. Neuropharmacology 38:467–475.

Dutar P, Petrozzino JJ, Vu HM, Schmidt MF, Perkel DJ (2000) Slow synaptic inhibition mediated by metabotropic glutamate receptor activation of GIRK channels. J Neurophysiol 84:2284–2290.

Feldmeyer D, Egger V, Lubke J, Sakmann B (1999) Reliable synaptic connections between pairs of excitatory layer 4 neurones within a single "barrel" of developing rat somatosensory cortex. J Physiol (Lond) 521:169–190.

Fortune ES, Margoliash D (1995) Parallel pathways and convergence onto HVc and adjacent neostriatum of adult zebra finches (*Taeniopygia guttata*). J Comp Neurol 360:413–441.

Foster EF, Bottjer SW (1998) Axonal connections of the high vocal center and surrounding cortical regions in juvenile and adult male zebra finches. J Comp Neurol 397:118–138.

Gahr M, Garcia-Segura LM (1996) Testosterone-dependent increase of gap-junctions in HVC neurons of adult female canaries. Brain Res 712:69–73.

Galarreta M, Hestrin S (2002) Electrical and chemical synapses among parvalbumin fast-spiking GABAergic interneurons in adult mouse neocortex. Proc Natl Acad Sci USA 99:12438–12443.

Hahnloser RH, Kozhevnikov AA, Fee MS (2002) An ultra-sparse code underlies the generation of neural sequences in a songbird. Nature 419:65–70.

Hessler NA, Doupe AJ (1999) Singing-related neural activity in a dorsal forebrain–basal ganglia circuit of adult zebra finches. J Neurosci 19:10461–10481.

Johnson F, Bottjer SW (1993) Induced cell death in a thalamic nucleus during a restricted period of zebra finch vocal development. J Neurosci 13:2452–2462.

Katz LC, Gurney ME (1981) Auditory responses in the zebra finch's motor system for song. Brain Res 221:192–197.

Kirn JR, Alvarez-Buylla A, Nottebohm F (1991) Production and survival of projection neurons in a forebrain vocal center of adult male canaries. J Neurosci 11:1756–1762.

Konishi M (1965) The role of auditory feedback in the control of vocalization in the white-crowned sparrow. Z Tierpsychol 22:770–783.

Kubota M, Saito N (1991) Sodium- and calcium-dependent conductances of neurones in the zebra finch hyperstriatum ventrale pars caudale in vitro. J Physiol (Lond) 440:131–142.

Leonardo A (2002) Neural dynamics underlying complex behavior in a songbird. PhD thesis, California Institute of Technology.

Lewicki MS (1996) Intracellular characterization of song-specific neurons in the zebra finch auditory forebrain. J Neurosci 16:5855–5863.

Lewicki MS, Arthur BJ (1996) Hierarchical organization of auditory temporal context sensitivity. J Neurosci 16:6987–6998.

Lewicki MS, Konishi M (1995) Mechanisms underlying the sensitivity of songbird forebrain neurons to temporal order. Proc Natl Acad Sci USA 92:5582–5586.

Livingston FS, Mooney R (1997) Development of intrinsic and synaptic properties in a forebrain nucleus essential to avian song learning. J Neurosci 17:8997–9009.

Livingston FS, White SA, Mooney R (2000) Slow NMDA-EPSCs at synapses critical for song development are not required for song learning in zebra finches. Nat Neurosci 3:482–488.

Long MA, Landisman CE, Connors BW (2004) Small clusters of electrically coupled neurons generate synchronous rhythms in the thalamic reticular nucleus. J Neurosci 24:341–349.

Luo M, Perkel DJ (2002) Intrinsic and synaptic properties of neurons in an avian thalamic nucleus during song learning. J Neurophysiol 88:1903–1914.

Lytton WW, Sejnowski TJ (1991) Simulations of cortical pyramidal neurons synchronized by inhibitory interneurons. J Neurophysiol 66:1059–1079.

Maccaferri G, Roberts JD, Szucs P, Cottingham CA, Somogyi P (2000) Cell surface domain specific postsynaptic currents evoked by identified GABAergic neurones in rat hippocampus in vitro. J Physiol (Lond) 524:91–116.

Marder E, Bucher D (2001) Central pattern generators and the control of rhythmic movements. Curr Biol 11:R986–R996.

Margoliash D (1983) Acoustic parameters underlying the responses of

song-specific neurons in the white-crowned sparrow. J Neurosci 3:1039–1057.

Margoliash D, Fortune ES (1992) Temporal and harmonic combination-sensitive neurons in the zebra finch's HVc. J Neurosci 12:4309–4326.

Mooney R (1992) Synaptic basis for developmental plasticity in a birdsong nucleus. J Neurosci 12:2464–2477.

Mooney R (2000) Different subthreshold mechanisms underlie song selectivity in identified HVc neurons of the zebra finch. J Neurosci 20:5420–5436.

Mooney R, Konishi M (1991) Two distinct inputs to an avian song nucleus activate different glutamate receptor subtypes on individual neurons. Proc Natl Acad Sci USA 88:4075–4079.

Nambu A (2004) A new dynamic model of the cortico-basal ganglia loop. Prog Brain Res 143:461–466.

Nixdorf BE (1989) Ultrastructural analysis of the development and maturation of synapses and subsynaptic structures in the ectostriatum of the zebra finch. J Comp Neurol 290:472–486.

Nottebohm F, Stokes TM, Leonard CM (1976) Central control of song in the canary, *Serinus canarius*. J Comp Neurol 165:457–486.

Nottebohm F, Kelley DB, Paton JA (1982) Connections of vocal control nuclei in the canary telencephalon. J Comp Neurol 207:344–357.

Perkel DH, Gerstein GL, Moore GP (1967) Neuronal spike trains and stochastic point processes. I. The single spike train. Biophys J 7:391–418.

Pouille F, Scanziani M (2001) Enforcement of temporal fidelity in pyramidal cells by somatic feed-forward inhibition. Science 293:1159–1163.

Prather J, Mooney R (2003) Synaptic coupling of HVC neurons revealed by pairwise recordings. Soc Neurosci Abstr 29:294.11.

Price PH (1979) Developmental determinants of structure in zebra finch song. J Comp Physiol Psychol 93:260–277.

Rauske PL, Shea SD, Margoliash D (2003) State and neuronal class-dependent reconfiguration in the avian song system. J Neurophysiol 89:1688–1701.

Reiner A (2002) Functional circuitry of the avian basal ganglia: implications for basal ganglia organization in stem amniotes. Brain Res Bull 57:513–528.

Rosen MJ, Mooney R (2003) Inhibitory and excitatory mechanisms underlying auditory responses to learned vocalizations in the songbird nucleus HVC. Neuron 39:177–194.

Scharff C, Nottebohm F (1991) A comparative study of the behavioral deficits following lesions of various parts of the zebra finch song system: implications for vocal learning. J Neurosci 11:2896–2913.

Scharff C, Kirn JR, Grossman M, Macklis JD, Nottebohm F (2000) Targeted neuronal death affects neuronal replacement and vocal behavior in adult songbirds. Neuron 25:481–492.

Schmidt MF, Perkel DJ (1998) Slow synaptic inhibition in nucleus HVc of the adult zebra finch. J Neurosci 18:895–904.

Selverston AI, Moulins M (1985) Oscillatory neural networks. Annu Rev Physiol 47:29–48.

Sil'kis IG (2002) A possible mechanism for the dopamine-evoked synergistic disinhibition of thalamic neurons via the "direct" and "indirect" pathways in the basal ganglia. Neurosci Behav Physiol 32:205–212.

Theunissen FE, Doupe AJ (1998) Temporal and spectral sensitivity of complex auditory neurons in the nucleus HVc of male zebra finches. J Neurosci 18:3786–3802.

Troyer TW, Doupe AJ (2000) An associational model of birdsong sensorimotor learning I. Efference copy and the learning of song syllables. J Neurophysiol 84:1204–1223.

White SA, Livingston FS, Mooney R (1999) Androgens modulate NMDA receptor-mediated EPSCs in the zebra finch song system. J Neurophysiol 82:2221–2234.

Wichmann T, DeLong MR (1996) Functional and pathophysiological models of the basal ganglia. Curr Opin Neurobiol 6:751–758.

Wild JM, Williams MN, Howie GJ, Mooney R (2005) Calcium binding proteins define interneurons in HVC of the zebra finch (*Taeniopygia guttata*). J Comp Neurol 483:76–90.

Wilson CJ (1993) The generation of natural firing patterns in neostriatal neurons. Prog Brain Res 99:277–297.

Zuschratter W, Braun S, Scheich H (1987) Co-localization of parvalbumin, calbindin and GABA in avian vocal motor system. Neuroscience [Suppl] 22:S114.